Surface & Coatings Technology 218 (2013) 80–86

Contents lists available at SciVerse ScienceDirect

Surface & Coatings Technology

journal homepage: www.elsevier.com/locate/surfcoat

Optimization of sputtering parameters for Ni–Cr alloy deposition on copper foil as embedded thin film resistor

Lifei Lai [a,b,c], Wenjin Zeng [a], Xianzhu Fu [a], Rong Sun [a,*], Ruxu Du [d]

[a] Shenzhen Institutes of Advanced Technology, Chinese Academy of Sciences, Shenzhen 518055, PR China
[b] Graduate University of Chinese Academy of Sciences, Beijing 100049, PR China
[c] Ningbo University of Technology, Ningbo 315016, PR China
[d] The Chinese University of Hong Kong, Shatin, Hong Kong, PR China

ARTICLE INFO

Article history:
Received 8 July 2012
Accepted in revised form 22 December 2012
Available online 31 December 2012

Keywords:
Ni–Cr alloy
Magnetron sputtering
Embedded thin film resistor
Taguchi method

ABSTRACT

Ni–Cr (80/20 at.%) alloy was deposited on the copper foil substrate by DC magnetron sputtering process. Taguchi method was applied to optimize the deposition parameters including sputtering power, substrate temperature, and argon pressure. Sputtering power was found to be the most prominent factor that influenced the electrical properties of Ni–Cr alloy film by employing the range analysis. Embedded thin film resistor (ETFR) with a high resistivity of 6.69×10^{-4} Ω.cm and a low temperature coefficient of resistance of 374.78 ppm/K was obtained under the optimized deposition conditions. A feasible way was demonstrated to fabricate high-quality Ni–Cr alloy on copper foil as ETFR materials.

1. Introduction

With the miniaturization of electronic products, the integration density of passive components (PCS) is reaching its limit on the printed circuit board (PCB). One promising solution is to integrate PCS into PCB, which can save at least 40% space of PCB compared with the traditional surface mounted technique (SMT) and also yield a more reliable PCB by reducing the number of solder joints [1]. Embedded thin film resistor (ETFR), one of the PCS, can be made by sandwiching the thin film resistor between the copper foil and dielectric layer, and being pressed into PCB after etching. ETFR possesses many merits including good electrical performance, low cost and miniaturized packaging size, etc. [1,2]. Ni–Cr (80/20 at.%) alloy is usually used as ETFR materials due to its high reliability, high electrical resistivity and small temperature coefficient of resistance (TCR) [3–5]. The most common method is DC magnetron sputtering to fabricate Ni–Cr alloy thin film [6]. Ni–Cr alloy based on the substrates such as glass, silicon, ceramic and stainless steel has been widely used as sensor or chip resistor for common integrated circuit [4,7–10]. However, few studies have been reported about depositing Ni–Cr alloy on copper foil as ETFR materials. It should be noted that copper foil as a substrate plays an important role in 3D electronics packaging technology since it can be used as both multilayer core boards and electrode. Therefore it is necessary to investigate the process condition for the deposition of Ni–Cr alloy on copper foil.

In this work, the Taguchi design method was used to optimize the parameters of depositing Ni–Cr alloy on copper foil [11–13]. Orthogonal experiment scheme (L_9 (3^4)) was designed and three critical parameters were taken into account: sputtering power, argon pressure and substrate temperature. The best combination of deposition parameters was found by using the range analysis. The properties of ETFR were also evaluated.

2. Experimental

2.1. Materials and methods

Ni–Cr (80/20 at.%) alloy (99.99% purity) was used as target for sputtering. High purity Ar (99.999% purity) was introduced as the sputtering gas. Very low profile (VLP) electrolytic copper foil (18 μm thickness) was selected as substrate. To achieve good adhesion and large sheet resistance, the Ni–Cr thin films was deposited on matte side of copper foil by DC magnetron sputtering. Before sputtering, copper foil and float glass were ultrasonically cleaned in sequence by acetone, alcohol and deionized water, with 10 min for each step, respectively. The clean copper foil and float glass were transferred into the sputtering chamber after completely flowed dry by nitrogen gun. The gas flow was 80 sccm and the base pressure was 8.5×10^{-4} Pa. The sputtered time was set at 4 min. Before deposition, the alloy target was pre-sputtered for about 10 min to remove contaminants from the surface. After sputtering, the copper foil coated with Ni–Cr alloy was fixed on the core board by the epoxy of 106 prepreg (PP). 106 PP is a semi-curing sheet and becomes adhesive under the high temperature. The ETFR was obtained after brown oxidation, etching and laminating of the core boards [14].

* Corresponding author. Tel.: +86 755 86392158; fax: +86 755 86392299.
E-mail address: rong.sun@siat.ac.cn (R. Sun).

0257-8972/$ – see front matter © 2012 Elsevier B.V. All rights reserved.
http://dx.doi.org/10.1016/j.surfcoat.2012.12.030

An orthogonal scheme (L9 (3^4)) was carefully designed to organize the film depositions. Values of three typical control parameters, including sputtering power, argon pressure and substrate temperature, were determined through the orthogonal array. In order to analyze the thermal stability of ETFR, the ETFR was rapidly heated to 250 °C at a rate of 40 °C/min, then gradually cooled down at a rate of 20 °C/min by the detection probing station (HFSE-PB4). The sheet resistance of ETFR was measured using a digital source meter (Keithley 2410) with the step of 10 °C in the cooling process. The film thickness was determined by a calibrated surface profiler (Model XP-1). The microstructure and internal stress of ETFR were analyzed by XRD (X'pert PRO, NL). The surface morphology of ETFR materials was examined by AFM (CSPM5000) and SEM (Hitachi S-4800). The surface chemical state of ETFR material was investigated by XPS (ULVAC-PHI 1800) using a 1486.6 eV Al $k\alpha$ source, all binding energy values were compensated to C 1s (284.5 eV), the sputter rate is 8.0 nm min^{-1} for depth profiling by SiO_2 as the scale of standard sample and argon gas as the sputtering gas. The elemental concentrations of ETFR materials were detected by EDS (EMAX250).

2.2. The calculation of relevant parameters

Resistivity (ρ) is calculated from $\rho = R_s \times d$, where R_s is the sheet resistance and d is the film thickness. The thickness d of Ni–Cr alloy on the top of copper foil was determined by the alloy thickness on the top of float glass since the copper foil was too soft. The TCR is defined as $\mathrm{TCR} = \frac{(R_t - R_{t_0})}{R_{t_0}(t-t_0)} \times 10^6 (\mathrm{ppm/K})$, where R_{t_0} and R_t are the sheet resistance of ETFR measured at the temperature of t_0 (room temperature) and t, respectively, and the mean value of TCR was regarded as the final result.

The crystallite size was estimated by the Debye–Scherrer formula (1). The stress vertical film surface is calculated by formula (2) [15]:

$$L_{hkl} = \frac{k\lambda_{k\alpha 1}}{\beta_1 \cos\theta} \tag{1}$$

$$\sigma = \frac{E_f}{2\nu_f}\frac{d_0 - d}{d_0} \tag{2}$$

where L_{hkl} is the crystallite size, K is the correction factor (0.89), $\lambda_{k\alpha 1}$ is the X-ray wavelength (0.15406 nm), β_1 is the FWHM value, θ is the Bragg diffraction angle. σ is the stress, d_0 and d are the interplanar distance with or without stress, respectively. E_f is Young's modulus and ν_f is Poisson's ratio.

3. Results and discussion

3.1. Range analysis of sputtering parameters

Table 1 lists the three factors and their corresponding three different levels investigated in this work. Nine groups of experiments were carried out with varied levels of the three factors which were scheduled in Table 2. The resistivity and TCR of the ETFR are also indicated in Table 2. The range analysis values were presented in Table 3. R_j is defined as: $R_j = \max\{|K_{1j} - K_{2j}|, |K_{2j} - K_{3j}|, |K_{3j} - K_{1j}|\}$. K_{ij} is the mean value about the corresponding index of j column factor and i level, for example, K_{iA} is defined as: $K_{1A} = \frac{1}{3}\sum_{A_i = A_1}(A_i)$. Theoretically, the R_j value reflects the impact of the corresponding factor on the film properties. The impact degree will be larger as the R_j is greater. As shown in Table 3, the sputtering power is the factor that mostly affects the resistivity and TCR, while the argon pressure is the minimal impact factor. On the other hand, the K_{ij} value has the same change trends with the corresponding resistivity and TCR. As shown in the first row of Table 3, K_{1A} is the greatest in K_{iA}, so A1 will be selected for the highest resistivity among A1, A2 and A3. Similarly, K_{2B} and K_{1C} are the greatest in K_{iB} and K_{iC}, respectively, so B2 and C1 will be selected for the highest resistivity. Therefore, the combination for the highest resistivity is $A_1B_2C_1$. The level generating the smallest K_{ij} value in the last 3 rows of Table 3 are the combination for the smallest value of TCR. Therefore, the preliminary predicted optimum combination of the three sputtering parameters is $A_3B_3C_2$ for the smallest TCR.

However, it was hard for a Ni–Cr film to attain both the highest resistivity and the lowest value of TCR simultaneously in the theoretical analysis and experiment. Since the resistance stability is more important, the optimum combination of the three sputtering parameters should be chosen as $A_3B_3C_2$, i.e., the combination of the smallest value of TCR, the Group 9 in Table 2. The corresponding parameters are: sputtering power of 405 W, argon pressure of 0.85 Pa and substrate temperature of 100 °C.

Fig. 1(a) shows the resistivity variation with different sputtering factors. The change trends of film resistivity and sputtering power were the opposite. The variation slope of resistivity of the Ni–Cr film for A1 → A2 was much larger than the one for A2 → A3, although the increase of the sputtering power in the former case (from 112 to 200 W) was smaller than the latter one (from 200 to 405 W). This phenomenon was related to the film thickness which usually decreased with the sputtering power and could be explained by the Sondheimer theory [16]: as the film thickness is greater than the mean free path of an electron, the relationship between resistivity and film thickness can be described as $\rho = \rho_B(1 + \frac{3\lambda}{8t})$, where ρ_B is the bulk resistivity, λ is the mean free path of an electron, and t is the thickness of film. It can be seen from the formula that the change of resistivity ρ exhibits an opposite trend with the film thickness t. When t is small enough, ρ increases rapidly with the t reduction. In addition, other factors such as residual stress can also influence the

Table 1
Sputtering factors and the corresponding levels in this experiment.

	A	B	C
	Sputtering power (W)	Argon pressure (Pa)	Temperature (°C)
Level 1	112	0.55	25
Level 2	200	0.65	100
Level 3	405	0.85	200

Table 2
Orthogonal design and experiment results.

Exp. no.	Control factors			Thickness (nm)	Resistivity (10^{-4} Ω.cm)	TCR (ppm/K)
	A	B	C			
1	A_1	B_1	C_1	51.44	32.70	2546.11
2	A_1	B_2	C_2	66.36	34.19	3572.90
3	A_1	B_3	C_3	44.21	16.15	2254.85
4	A_2	B_1	C_2	45.24	8.85	1013.28
5	A_2	B_2	C_3	77.38	8.98	601.44
6	A_2	B_3	C_1	56.33	10.88	2917.18
7	A_3	B_1	C_3	101.14	4.27	2414.85
8	A_3	B_2	C_1	107.21	6.68	1420.72
9	A_3	B_3	C_2	162.61	6.69	374.78

Table 3
Analysis of range and optimal parameters.

Factors	K_{ij}			R_j	Optimal parameters
	K_{1j}	K_{2j}	K_{3j}		
A	27.68	9.57	5.88	21.81	A_1
B	15.27	16.62	11.24	5.38	B_2
C	16.75	16.58	9.80	6.96	C_1
A	2791.29	1510.63	1403.45	1387.84	A_3
B	1991.41	1865.02	1848.94	142.47	B_3
C	2294.67	1653.65	1757.05	641.02	C_2

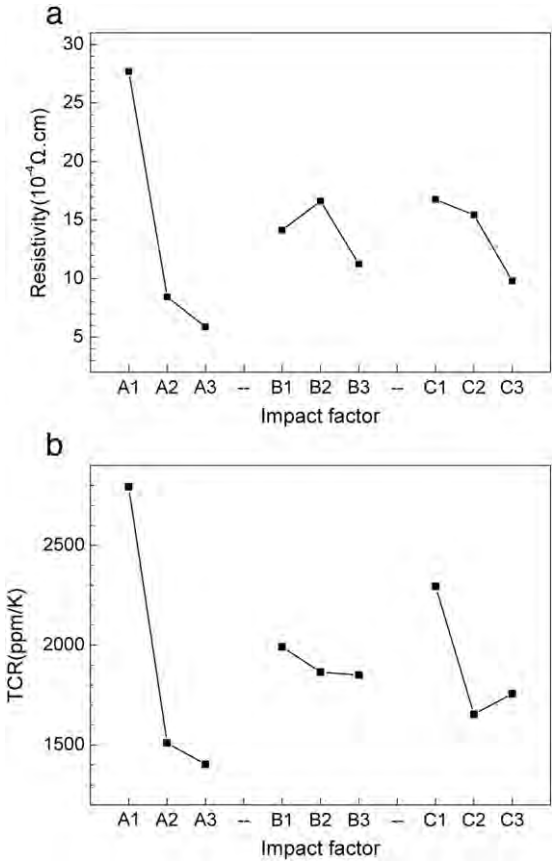

Fig. 1. Influence of sputtering parameters on Ni–Cr ETFR's electrical properties: (a) Resistivity, (b) TCR.

resistivity. It was found that there was an optimal argon pressure in B2 for the sputtering. Too high pressure could increase the discharge current and aggravate the backscattering effect, while too low pressure could influence the plasma generation [17]. As for the influence of substrate temperature, it was indicated that the resistivity had opposite changes with substrate temperature from C1 to C3. According to Mattiessen's formula [18]: $\rho_T = \rho_{Th} + \rho_I + \rho_D$, where ρ_T is total resistivity of the film. ρ_{Th}, ρ_I and ρ_D are the thermal, impurity and defect resistivity, respectively. ρ_I could be neglected here since we used high pure NiCr alloy. The resistivity of films deposited in the temperature range of 25–200 °C should be affected by defect scattering during carrier movement, thus the resistivity decreased with the increasing temperature [19].

Fig. 1(b) shows the trend of TCR variation with different sputtering factors. The TCR of A3 was the smallest among the factors. TCR decreased first quickly and then slowly, when the sputtering power increased from A1 to A2, and then to A3. Too low sputtering power would make the film structure loose and cause the lattice defects, resulting in unstable resistance and large TCR. Too large sputtering power would increase film stress, also resulting in large TCR. Argon pressure can affect the energy of sputtered metal atom, and influence the formation of crystal nucleus. As seen from the figure, TCR decreased slowly when argon pressure increased from B1 to B3. The smallest TCR was attained under the argon pressure of 0.85 Pa, i.e. B3. Substrate temperature had a significant effect on TCR. The lower substrate temperature (C1) caused more defects and the higher temperature (C3) led to larger residual stress. The TCR was the smallest at 100 °C, i.e. C2.

3.2. Microstructure and residual stress

Three groups of ETFR in Table 2 were selected for XRD testing according to their different TCR, including samples 2, 5 and 9. The diffraction peaks of Ni (011), Ni (002), Cr (110) and Cr (200) are observed in Fig. 2. Ni (011) peak and Cr (110) peak were almost coincident, and main strong peaks should be both combined peaks. Sample 5 was the strongest intensity peak, which suggested that a high substrate temperature benefited the crystallization of metal atoms. From the Ni–Cr alloy phase diagram [20], it is known that there was mainly a Ni single-phase solid solution when the Cr concentration was 20% and the temperature was less than 1200 °C, so the Ni–Cr intermetallic compound did not exist. The broad diffraction peak suggests that the Ni–Cr thin film was composed of a crystalline one and an amorphous one. Table 4 shows the grain sizes of three samples along Ni (011). The grain size of sample 2 was the smallest. According to the general characteristics of metal and alloy, the grain boundary would be bigger as the grain is smaller [21,22]. The resistivity would enhance as the charge carrier scattering at grain boundary increases. The stress of samples along Ni (011) is also presented in Table 4, all of them are tensile stress. The stress of sample 2 was the largest, while sample 9 was the smallest. The resistivity of thin film increased with the increase of residual stress since the gathering strain energy could reinforce the grain boundary distortion [23,24]. In addition, thin film with large stress is easy to break which leads to an unstable resistance, i.e. high TCR. Sample 2 exhibited the smallest crystal grain and the strongest stress, thus its resistivity and TCR were the biggest. While the grain size of sample 9 was smaller than sample 5, but its stress was the smallest among them, so it possessed the lowest TCR among the three samples. Therefore the XRD results proved that Group 9 was the optimal parameter.

3.3. Surface morphology

Fig. 3 displays the three-dimensional AFM image of samples 2, 5 and 9 in a scanning area of 20 μm × 20 μm. The surface morphology of the samples was different. The surface particles of sample 2 were obviously inconsistent. The grain average diameters of samples 2, 5 and 9 were 650 nm, 510 nm and 989 nm, respectively. The surface root-mean-square (RMS) roughness of samples 2, 5 and 9 were about 161 nm, 178 nm and 113 nm, respectively. The particles of sample 9 were arranged closely due to the large particles and low surface roughness.

SEM surface images of samples 2, 5 and 9 are shown in Fig. 4(a), (b) and (c), respectively. It could be observed from Fig. 4 that the gaps between the particles of sample 2 were the largest compared to these of samples 5 and 9. Fig. 4(b) shows a more uniform particle size of sample 5, indicating its good crystallinity, which was consistent with the XRD analysis in Fig. 2. Fig. 4(c) shows that the combination of particles of sample 9 was the most close, indicating that the defects of sample 9 were less, thus it exhibited more stable electrical properties among the three samples.

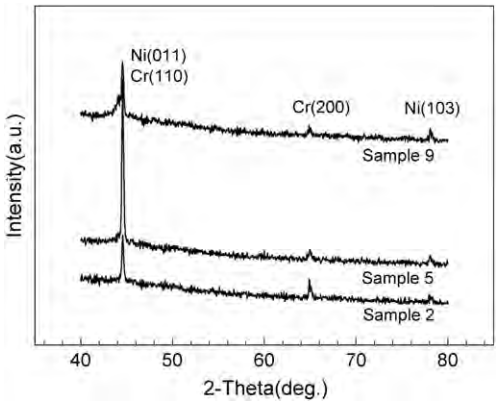

Fig. 2. XRD patterns of Ni–Cr ETFR samples.

Table 4
The XRD patterns of the chosen Ni–Cr ETFR samples (Ni (0 1 1) peak).

No.	h k l	d($\times 10^{-1}$ nm)	2θ (°)	Δd (nm)	FWHM (°)	Crystallite size (nm)	Stress (MPa)
2	0 1 1	2.0311	44.574	0.0023	0.327	25.9	386.4
5	0 1 1	2.0317	44.559	0.0017	0.189	44.9	285.9
9	0 1 1	2.0319	44.556	0.0015	0.305	27.8	252.2

3.4. Electrical properties

Fig. 5(a) shows the temperature dependence of sheet resistance of samples 2, 5 and 9 from room temperature to 250 °C. The sheet resistance of sample 2 was the largest among the three samples, but there were some fluctuations in sample 2 at different temperatures. The sheet resistances of samples 9 and 5 decreased slightly as the temperature dropped, reflecting the thermal property of metal. The variation of the TCR of samples 2, 5 and 9 with temperature is presented in Fig. 5(b). The TCR of sample 9 became stable when the temperature was higher than 50 °C while the TCR of sample 2 showed a large fluctuation, especially when the test temperature was below 80 °C. Compared with sample 9, the TCR of sample 5 was unstable between 50 °C and 100 °C. Fig. 5(c) shows the temperature dependence of the TCR of the nine groups of samples in the orthogonal experiment scheme, and the TCR of sample 9 has the smallest fluctuation among them. Therefore, sample 9 had the best electrical property.

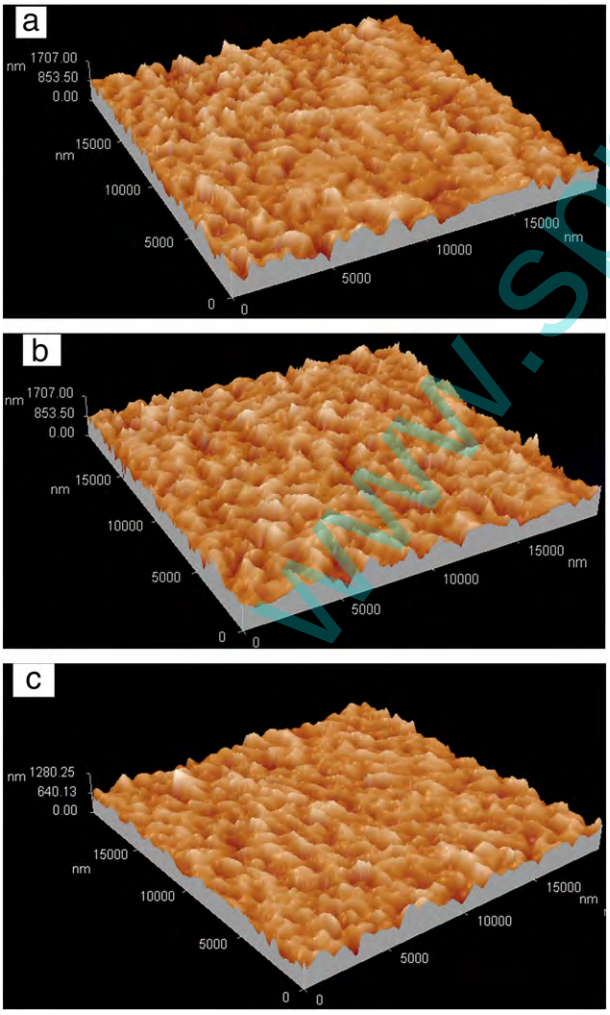

Fig. 3. AFM images of Ni–Cr ETFR materials: (a) sample 2, (b) sample 5, (c) sample 9.

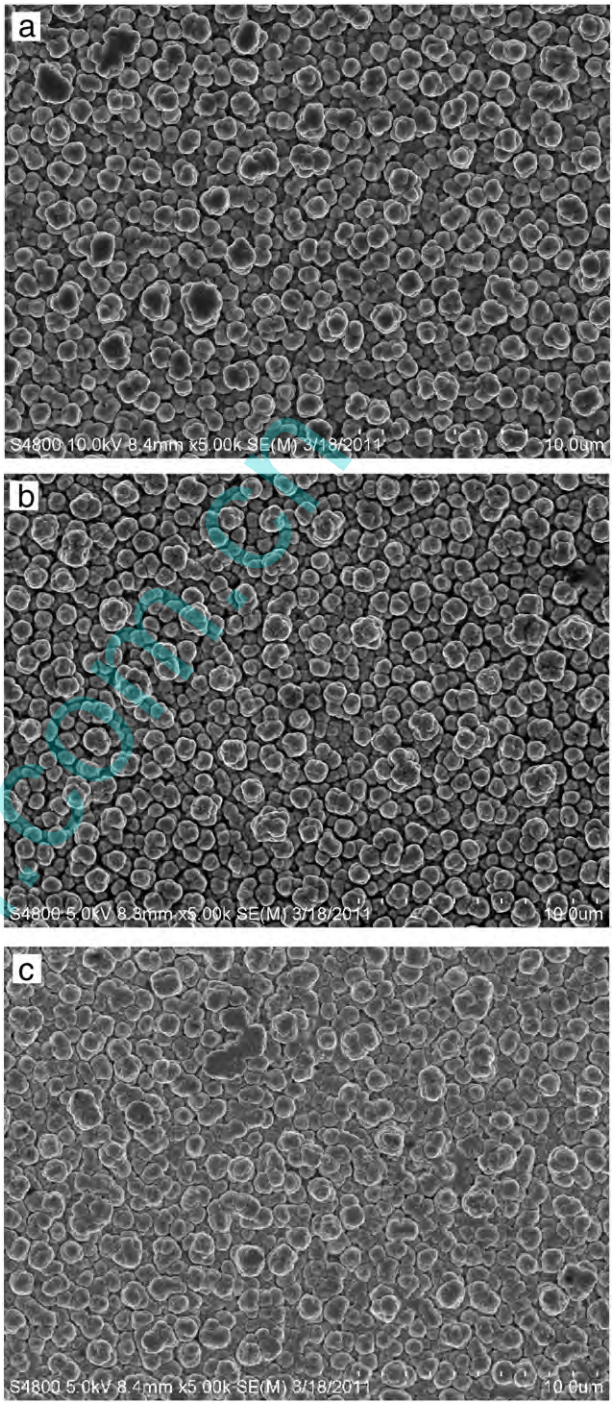

Fig. 4. SEM surface images of Ni–Cr ETFR materials: (a) sample 2, (b) sample 5, (c) sample 9.

In order to further testify the temperature dependence of the TCR of the optimized Ni–Cr ETFR, the temperature range was chosen to be −50 °C to 250 °C. Fig. 6 presents the temperature dependence of the TCR under optimal sputtering conditions by changing sputtering power, argon pressure and substrate temperature, respectively. Only the sputtering power changed under optimal sputtering condition is shown in Fig. 6(a). The sputtering power was selected at 80 W, 202 W, 405 W and 600 W, respectively. It is found that the fluctuation of TCR was large, whether at a low power 80 W or at a high power 600 W. The TCR at sputtering power of 405 W was the smallest among them. Only the argon pressure changed under the optimal sputtering condition is shown in Fig. 6(b). The argon pressure

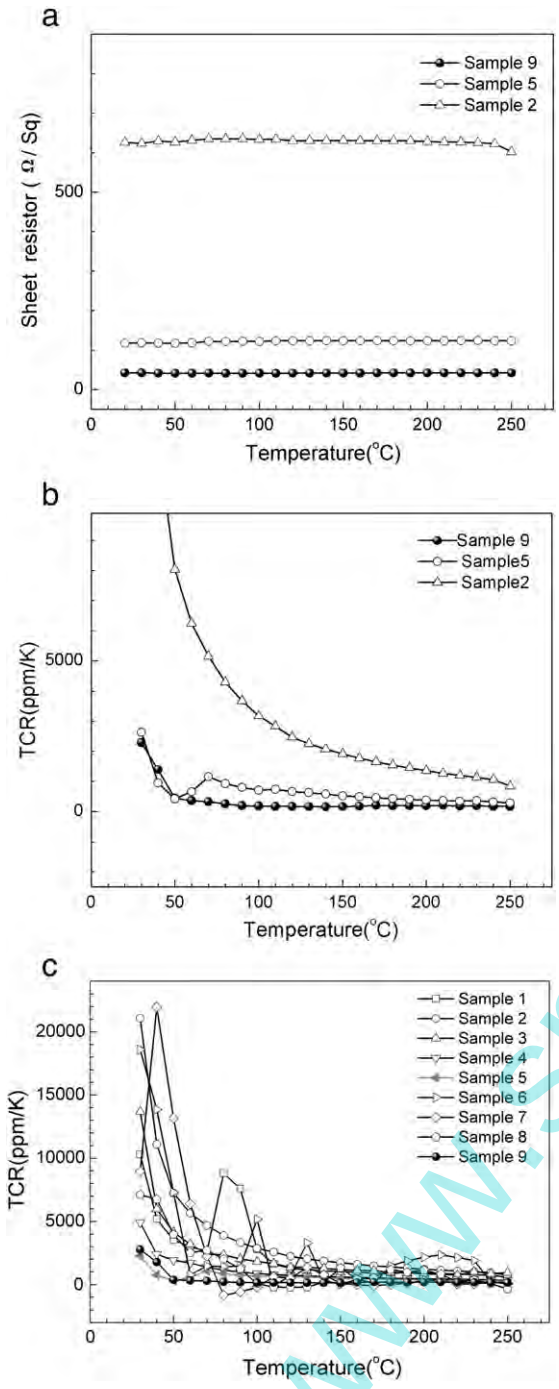

Fig. 5. The temperature dependence of the sheet resistor and the TCR of samples 2, 5 and 9: (a) sheet resistor, (b) TCR, (c) TCR of nine groups samples in the orthogonal array.

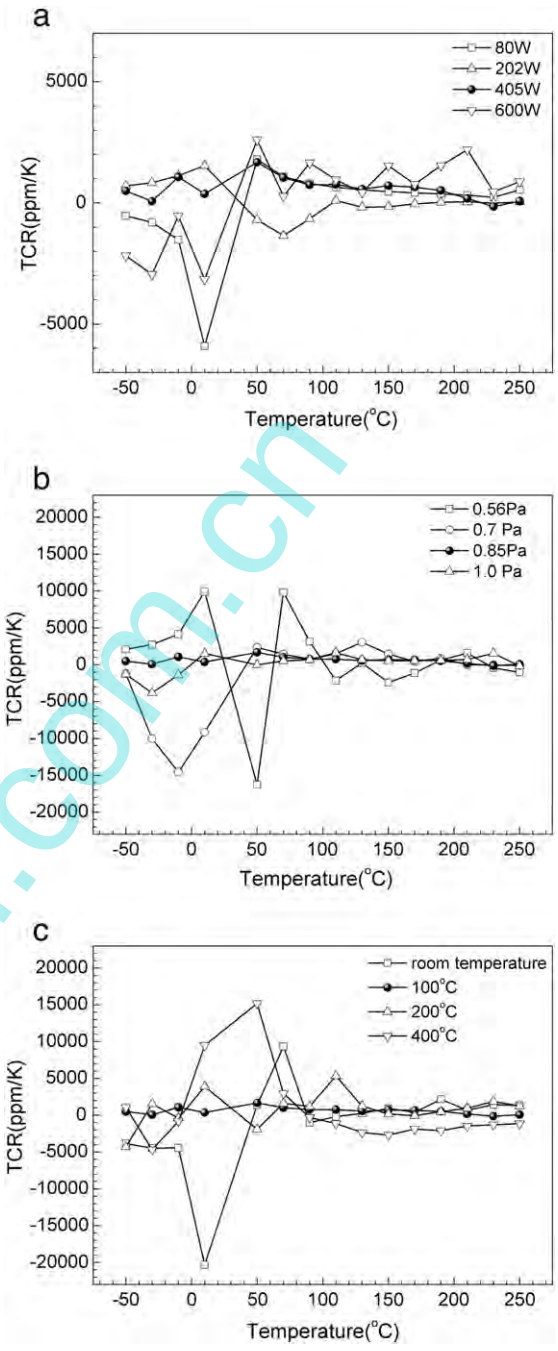

Fig. 6. The temperature dependence of the TCR under optimal sputtering condition: (a) sputtering power, (b) argon pressure, (c) substrate temperature.

selected was 0.56 Pa, 0.70 Pa, 0.85 Pa and 1.0 Pa, respectively. It is found that the fluctuation of TCR is large in 0.56 Pa and 0.7 Pa. The TCR in 0.85 Pa argon pressure was the smallest among them. Only the substrate temperature changed under the optimal sputtering condition is shown in Fig. 6(c). The substrate temperature was selected at room temperature, 100 °C, 200 °C and 400 °C, respectively. It is found that the fluctuation of TCR was large, whether at the room temperature or at a high temperature 400 °C. The TCR at 100 °C was smallest among them. These reasons had been explained by TCR variation trend with different sputtering factors in Fig. 1(b). So the sputtering parameter set for sample 9 was the best experimental parameter.

3.5. Composition

XPS analysis was performed to identify the surface component of the optimal samples, i.e., sample 9. Fig. 7(a) shows the narrow scan spectra of $Ni2p_{3/2}$ on the ETFR material surface. Ni-metal and Ni $(OH)_2$ were detected at binding energies of 852.24 and 855.37 eV, respectively. A small amount of NiO (854.74 eV) was also detected in overlapped peaks. And the O1s peaks at 530.80 and 530.05 eV in Fig. 7(c) were corresponded to Ni $(OH)_2$ and NiO, respectively. The Ni metal was the main component on the surface of ETFR. Fig. 7(b) shows that the peak of $Cr2p_{3/2}$ can be fitted by two Gaussian peaks. The binding energy of the main peak was 576.28 eV, and the smaller peak was 574.6 eV, which corresponded to those of Cr^{+3} and Cr metal, respectively [25,26]. The predominant component for Cr on

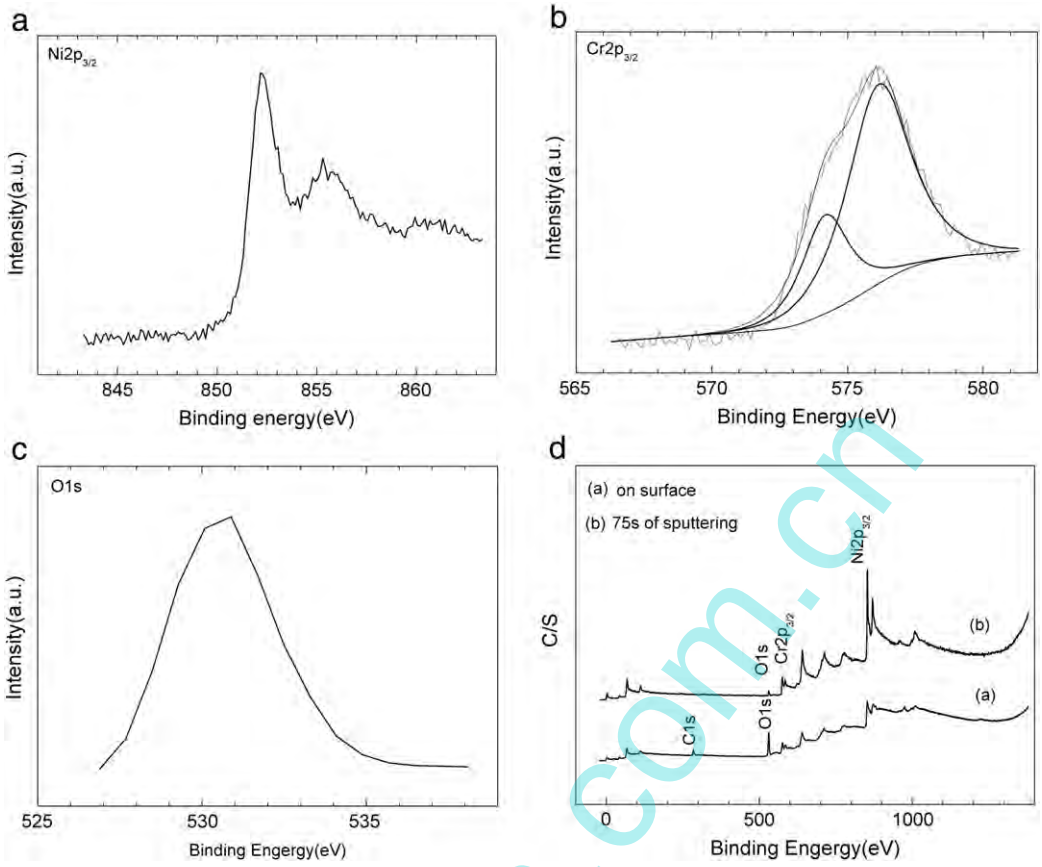

Fig. 7. XPS spectra of Ni–Cr ETFR materials deposited under optimal conditions: (a) $Ni2p_{3/2}$ (b) $Cr2p_{3/2}$ (c) O1s, (d) XPS full spectrum of the Ni–Cr film surface and after 75 s of sputtering.

the ETFR surface was Cr_2O_3. Fig. 7(d) shows the full XPS spectra from the surface and bulk of the Ni–Cr film prepared by sputtering for 75 s. It can be seen that the oxygen content was reduced from the smaller O1s peak spectrum by sputtering, indicating that pure Ni and Cr were mainly distributed in the bulk of the ETFR material.

Fig. 8 shows the EDS analysis of the optimal Ni–Cr ETFR samples. Ni and Cr contents in the thin film were 10.40 at.% and 3.01 at.%, respectively. It can be found that the concentration ratio of Ni and Cr in thin film was 3.46, closing to the NiCr atomic ratio in the target, which suggested that the magnetron sputtering method can keep the composition stability of the ETFR materials. The 62.16 at.% C element, 19.42 at.% O element and 5.01 at.% Br element in EDS results mainly came from the epoxy resin in the core boards and 106 PP. The core board and the106 PP were the components of ETFR [14].

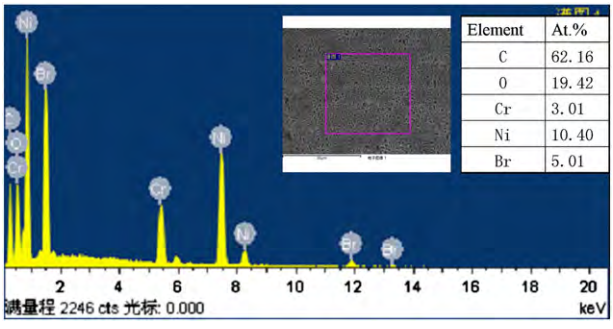

Fig. 8. EDS analysis for the optimal Ni–Cr ETFR samples.

4. Conclusions

Ni–Cr thin film for embedded resistor was obtained by DC magnetron sputtering process. The influence of process parameters (including sputtering power, argon pressure and substrate temperature) on the resistivity and TCR of Ni–Cr ETFR were investigated by Taguchi method. The sputtering power was the most prominent factor which significantly influenced the resistivity and TCR of the Ni–Cr ETFR. The optimized deposition parameters were: sputtering power of 405 W, argon pressure of 0.85 Pa, and substrate temperature of 100 °C. Ni–Cr ETFR deposited under the optimized conditions exhibited a high resistivity of 6.69×10^{-4} Ω.cm and a low TCR of 374.78 ppm/K.

Acknowledgments

The authors thank the financial support of the National Natural Science Foundation of China (No. 20971089), research funding from the National S&T Major Project (No. 2009ZX02038) and the Guangdong Innovative Research Team Program (No. 2011D052).

References

[1] J. Wang, R. Hilburn, S. Clouser, B. Greenlee, Proceedings of the IPC Annual Meeting, Louisiana, U.S.A., November, 2002, 2002, p. S03.
[2] G. Min, Synth. Met. 153 (2005) 49.
[3] J. Wang, S. Clouser, Proceedings of the IPC Printed Circuits EXPO, California, U.S.A., April, 2001, 2001, p. S08-1.
[4] I.H. Kazi, P.M. Wild, T.N. Moore, M. Sayer, Thin Solid Films 433 (2003) 337.
[5] E. Çadırlı, J. Non-Cryst. Solids 357 (2011) 809.
[6] L.F. Lai, R. Sun, T. Zhao, X.L. Zeng, S.H. Yu, International Symposium on APM, Xiamen, China, October, 2011, 2011, p. 60.
[7] W.S. Epling, G.B. Hoflund, Thin Solid Films 292 (1997) 236.
[8] E. Schippel, Thin Solid Films 144 (1986) 21.
[9] J.W. Yan, J.C. Zhou, Int. J. Mod. Phys. B 21 (2007) 4561.

[10] S. Vinayak, H.P. Vyas, K. Muraleedharan, V.D. Vankar, Thin Solid Films 514 (2006) 52.
[11] F. Wirbeleit, J. Non-Cryst. Solids 262 (2000) 207.
[12] W.L. Liu, S.H. Hsieh, W.J. Che, J.H. Lee, Surf. Coat. Technol. 201 (2007) 9238.
[13] G.C. Ji, C.J. Li, Y.Y. Wang, W.Y. Li, Surf. Coat. Technol. 200 (2006) 6749.
[14] H.F. Lee, C.Y. Chan, C.S. Tang, J. Mater. Process. Technol. 207 (2008) 72.
[15] L.Y. Yang, W.D. Guan, Z.M. Gu, Material Surface Film Technology, 1st ed. China Communications Press, Beijing, 1991.
[16] E.H. Sondheimer, Adv. Phys. 1 (1952) 1.
[17] Y.Ch. Zhang, Vacuum Coating Technology, 1st ed. Metallurgical Industry Press, Beijing, 2009.
[18] G.W.A. Dummer, Materials for Conductive and Resistive Function, Hayden Book Company Inc., New York, 1970.
[19] Y.M. Lu, W.S. Hwang, J.S. Yang, Surf. Coat. Technol. 155 (2002) 231.
[20] J. Rölke, Electrocompon. Sci. Technol. 9 (1981) 51.
[21] J.R. Ghosh, D. Basak, S. Fujihara, J. Appl. Phys. 96 (2004) 2689.
[22] S. Ebrahimiasl, W.M.Z.W. Yunus, A. Kassim, Z. Zainal, Solid State Sci. 12 (2010) 1323.
[23] A.F. Burnett, J.M. Cech, J. Vac. Sci. Technol. A 11 (1993) 2970.
[24] W.T. Tseng, Y.L. Wang, J. Niu, Thin Solid Films 370 (2000) 96.
[25] S.D. Yim, I.S. Nam, J. Catal. 221 (2004) 601.
[26] O. Nishimura, K. Yabe, M. Iwaki, J. Electron. Spectrosc. Relat. Phenom. 49 (1989) 335.